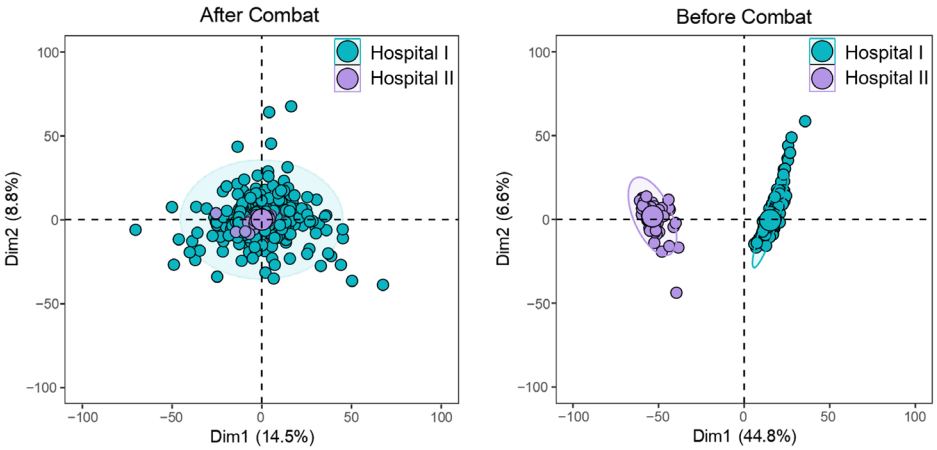


**Figure S1** PCA scatter plot. The first two principal components of the significant radiomic features were visualized in a two-dimensional scatter plot before and after using ComBat. The X and Y axes present the two principal component dimensions. Green and purple colors represent the two hospitals (Hospital I: Zhejiang Provincial People's Hospital, Hospital II: Hangzhou Traditional Chinese Medicine Hospital). PCA, principal component analysis.

**Table S1** Association between pericarotid fat density and the progression of CSVD

| PFD value | Without CSVD (n=34) | With CSVD without progression (n=83) | With CSVD progression (n=146) | P value |
|---|---|---|---|---|
| Mean (HU) | −62.34±7.67* | −57.19±7.31*# | −51.38±7.35# | <0.001 |
| Maximum (HU) | −42.08±4.75* | −39.22±4.67*# | −34.69±4.31# | <0.001 |
| Minimum (HU) | −83.83±13.33* | −75.17±11.33*# | −67.15±11.92# | <0.001 |

Data are presented as mean ± SD. For PFD value, *without CSVD *vs.* with CSVD without progression, P<0.01; #with CSVD without progression *vs.* with CSVD progression, P<0.01. PFD, pericarotid fat density; CSVD, cerebral small vessel disease; HU, Hounsfield Unit; SD, standard deviation.


https://dx.doi.org/10.21037/qims-24-1512

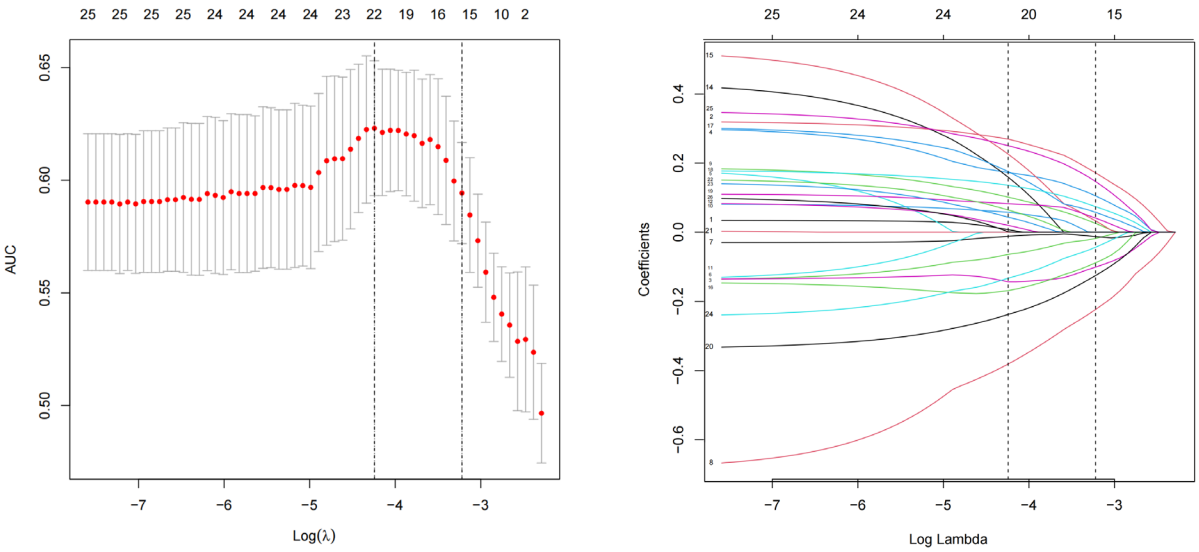


**Figure S2** Selection of radiomics signatures for the prediction models. (A) PVAT signatures selection by elastic logistic regression with the optimal penalization coefficient lambda (λ) using 10-fold cross-validation and the minimal criteria process. The X-axis shows Lambda (λ), and the Y-axis shows the model AUC. (B) Elastic Logistic Regression coefficient profile of the PVAT signatures. PVAT, perivascular adipose tissue.

**Table S2** Model coefficients of radiomic features

| Features | Coefficient | OR |
|---|---|---|
| L_wavelet.LHL_gldm_DependenceNonUniformityNormalized | −0.22311 | 0.800029 |
| R_original_shape_Maximum2DDiameterColumn | −0.12512 | 0.882387 |
| L_wavelet.LLH_glrlm_ShortRunLowGrayLevelEmphasis | −0.10079 | 0.904125 |
| L_wavelet.HLL_gldm_DependenceVariance | −0.08831 | 0.915481 |
| R_wavelet.HHL_glrlm_RunVariance | −0.04321 | 0.957714 |
| L_wavelet.LLH_firstorder_Skewness | −0.01749 | 0.982659 |
| L_wavelet.LHL_glcm_Idn | −0.01248 | 0.987602 |
| L_wavelet.LHL_glszm_SizeZoneNonUniformityNormalized | 0.025514 | 1.025842 |
| L_wavelet.HLL_glcm_Correlation | 0.032839 | 1.033384 |
| L_wavelet.LLL_glszm_SmallAreaEmphasis | 0.04101 | 1.041863 |
| L_wavelet.HLH_firstorder_Skewness | 0.057549 | 1.059237 |
| L_wavelet.HLH_glszm_GrayLevelNonUniformityNormalized | 0.074142 | 1.07696 |
| L_wavelet.LLH_glcm_ClusterTendency | 0.105067 | 1.110786 |
| R_wavelet.HHH_glszm_SizeZoneNonUniformityNormalized | 0.146488 | 1.157761 |
| L_original_glszm_SmallAreaLowGrayLevelEmphasis | 0.171797 | 1.187436 |


https://dx.doi.org/10.21037/qims-24-1512